Ka-Band Waveguide Phase Shifter Using Tunable Electromagnetic Crystal Sidewalls

J. Aiden Higgins, Hao Xin, *Member, IEEE*, A. Sailer, and Mark Rosker

***Abstract*—Tunable electromagnetic crystal (EMXT) structures have been used as sidewalls in special waveguides for frequencies of 30–40 GHz. This has the effect of substituting tunable impedance surfaces in place of the normal conducting metal sidewalls. The resulting EMXT waveguide boundary conditions can then be controlled *in situ* to achieve desired phase shifting and/or field flattening effects. Proof-of-concept experiments have been done using fix-tuned EMXT sidewalls with various resonant frequencies, and the measurements indicate that the insertion loss is low. An InP quantum barrier varactor approach is used to implement the tunable Ka-band EMXT waveguide phase shifter. The dependence of transmission amplitude and phase on the center frequency of sidewall resonance has been simulated and measured. Measurements and simulation results agree very well. The loss mechanism of the demonstrated phase shifter is well understood. Our results indicate that tunable EMXT waveguide will provide simple and low-loss phase-shifting systems.**

***Index Terms*—Electromagnetic crystal (EMXT), phase shifter, waveguide.**

I. Introduction

THE electromagnetic crystal (EMXT) considered here is a new type of periodic metallic electromagnetic (EM) structure that provides an artificial high-impedance surface boundary over a bandwidth centered at a resonance frequency $F_{\rm res}$. This kind of surface can provide very useful EM boundary conditions in many microwave and millimeter-wave applications including antenna ground planes [1]–[3], TEM waveguides [4], [5], filters [6], [7], etc. In particular, an EMXT with a tunable resonance frequency may have great potential in modern systems requiring agility and intelligence [8], [9].

Phase-shifting devices at microwave and millimeter-wave frequencies are extremely important in many military and commercial systems such as radar and communications. A novel type of waveguide phase shifter based on tunable EMXT surfaces has been developed and it may be particularly useful for millimeter-wave array systems tasked to provide agile beam steering. The new waveguide system is a rectangular waveguide in which the sidewalls have been replaced by tunable EMXT. EMXT presents a variable impedance surface at the sidewall in place of the normal perfect conductor sidewall. Prior realizations of this type of guide with fixed high-impedance sidewall surface have demonstrated, at Ku-band, that the electric field is made uniform across the guide width and that the insertion losses were low at Ku-band [10]. In this paper, the design and experimental results of a novel Ka-band phase-shifting waveguide using tunable EMXT sidewalls will be described. Tunable EMXT waveguide that can achieve polarization switching (i.e., linear to circular or vice versa) will also be proposed.

Manuscript received November 14, 2002.
The authors are with the Rockwell Scientific Company, Thousand Oaks, CA 91360 USA (e-mail: hxin@rwsc.com).
Digital Object Identifier 10.1109/TMTT.2003.809634

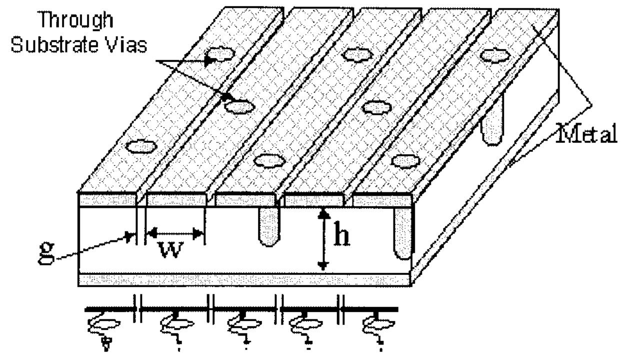

Fig. 1. Physical form of the strip-EMXT structure.

II. EMXT Surface

A. Fixed EMXT Surface

The initial high-impedance surfaces developed by Sievenpiper [2] were of a type that presented a surface that reflects an EM wave, incident at normal, with a reflection coefficient of nearly $+1\angle 0^\circ$ over the band of interest. This reflection coefficient was insensitive to the direction of the E-field polarization. Their effect of converting the TE10 guide mode into a TEM guide mode was demonstrated in the Ku-band waveguide [10]. The polarization-sensitive EMXT surfaces of this study are composed of a thin dielectric substrate that is metallized completely on one side (the "outside" of a waveguide) and has strips of metal separated by narrow gaps on the other side (the "inside" of a waveguide). This structure is shown in Fig. 1.

The substrate may be any low-loss microwave substrate. The gap g provides a capacitance that is part of a parallel resonant circuit. The substrate thickness h and the stripe width w provide an inductance that is effectively in parallel with the gap capacitance. An incident EM wave with an E-field across the strip will be coupled across the parallel resonant circuit. At the resonant frequency $F_{\rm res}$, the incoming wave is reflected with a $+1.0\angle 0^\circ$ coefficient. The orthogonal wave, with an E-field along the strips, is reflected as by a normal metal $(+1.0\angle 180^\circ)$.

Fig. 2 shows the measured reflection response for a polarization-sensitive strip-EMXT surface with a resonant frequency of 34.6 GHz. At the resonance frequency $F_{\rm res}$, the EMXT behaves like an open circuit to an incident wave. For frequency much

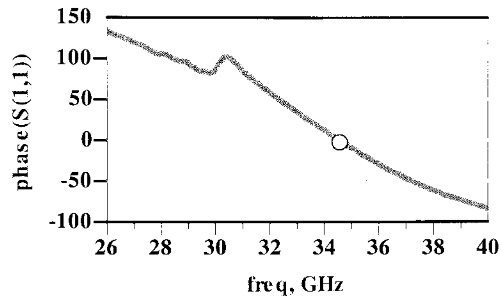

(a)

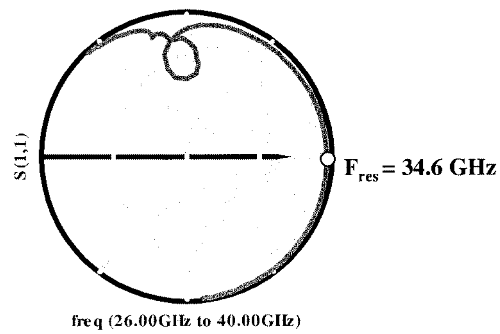

(b)

Fig. 2. (a) Reflection phase and (b) coefficient of an EMXT surface with a resonance frequency of 34.6 GHz. The EMXT substrate is Rogers Duroid 3006 with a dielectric constant 6.15 and loss tangent of 0.013. It has the following geometry: $g = 150\ \mu$m, $w = 356\ \mu$m, $h = 635\ \mu$m, via diameter $= 200\ \mu$m, and via periodicity $=$ 1270 μm.

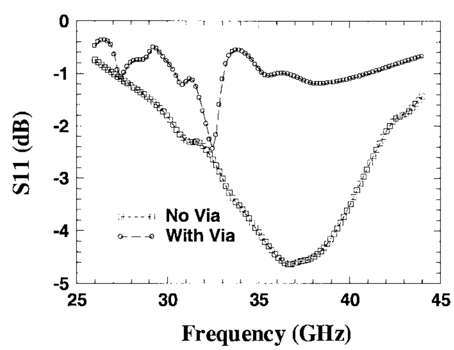

Fig. 3. HFSS simulated reflection loss of EMXT surfaces with and without through substrate vias. The geometry of the simulated EMXT is the same as that in Fig. 2.

lower or higher than F_{res}, the equivalent tank circuit in Fig. 1 presents a low impedance, and the EMXT response to an incoming wave approaches that of a perfect conducting metal.

Substrate vias (Fig. 1) were essential for this kind of EMXT surface to suppress the presence of substrate modes. It is worth mentioning that substrate vias are not necessary to provide inductance. Fig. 3 shows HFSS[1] simulated reflection magnitudes of a finite-size EMXT surface (same geometry as the sample shown in Fig. 2) with and without substrate vias. The resonant frequencies F_{res} for both cases are almost the same. However, it can be observed that, without substrate vias, power loss through substrate modes is quite high and the EMXT becomes impractical for most applications. EMXT without substrate vias has also been fabricated and high power loss associated with substrate modes was confirmed. Even though the installation of vias mitigates losses due to substrate modes, it does not eliminate them completely. For example, substrate-mode effects are apparent in Fig. 2 (measurement) and Fig. 3 (simulation) around 30 and 32 GHz, respectively. Since substrate modes in EMXT structures may cause significant losses, special care must be taken while designing EMXT-related applications. In fact, the unwanted substrate mode is a well-documented [11], [12] and analyzed phenomenon and can exist in the substrate as either TM or TE modes. For TM modes, the E-fields have components normal to the substrate plane and in the direction of propagation. For TE modes, the E-fields are parallel to the substrate plane and have no component in the direction of propagation. Analysis of the behavior of the substrate waves was performed using expressions from Kaminow *et al.* [12].

[1]*HFSS*, ver. 8, Ansoft Corporation, Santa Rosa, CA, 2001

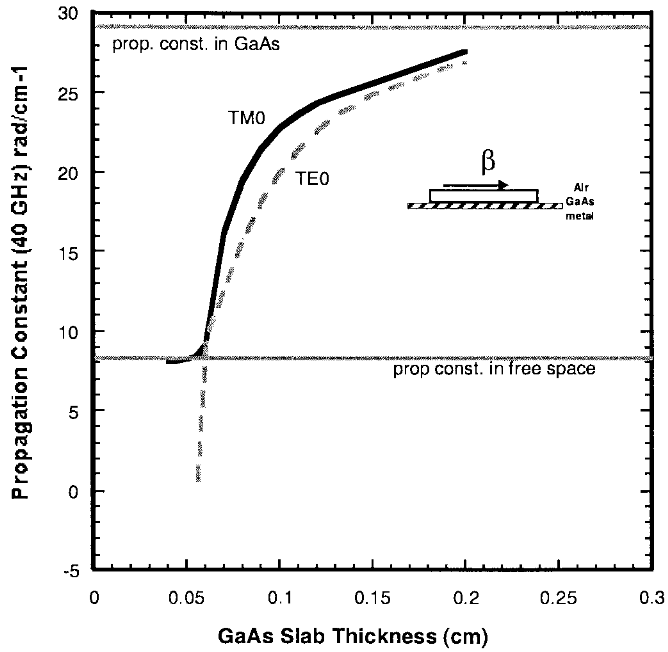

Fig. 4. Propagation constants of surface-mode waves in a substrate of GaAs with metal clad on one side at 40 GHz. The TM_0 mode always exists and properly distributed substrate vias can be used to suppress this mode.

The propagation constants of the TM_0 and TE_0 modes are illustrated in Fig. 4. These results, for the case of a GaAs substrate with metal clad on one side, are presented as a function of the substrate thickness at a frequency of 40 GHz. The results show that the TE_0 mode (and all other higher modes not shown) is subject to a cutoff as the substrate thickness decreases. Below 0.6 mm, these modes are cut off and only the TM_0 mode can persist. With smaller substrate thickness, its wavelength approaches asymptotically the wavelength in free space and the attenuation increases. For very thin substrates, the TM_0 mode exhibit the behavior of a "surface plasmon" wave. The substrate vias, present in sufficient numbers and properly spaced, will suppress this TM_0 mode.

Useful bandwidth is also an important parameter of EMXT surfaces. It depends on the design of the EMXT structure, particularly the thickness h. To the first order, EMXT bandwidth increases when the substrate is thicker. This is easily understand-

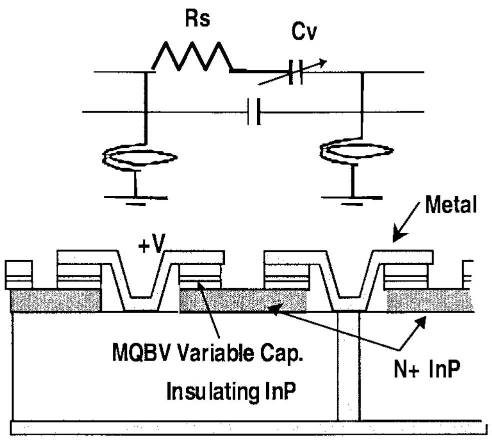

Fig. 5. Cross-sectional view and equivalent circuit of a monolithically integrated gap varactor for a tunable EMXT.

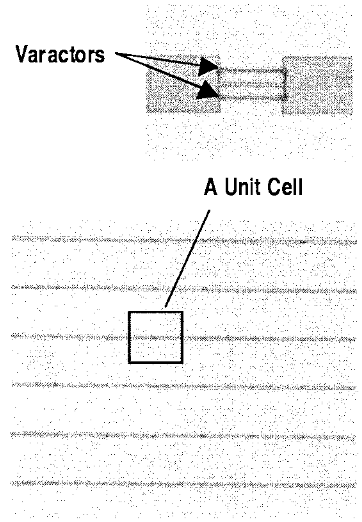

Fig. 6. Fabricated tunable EMXT based on InP TQBVs.

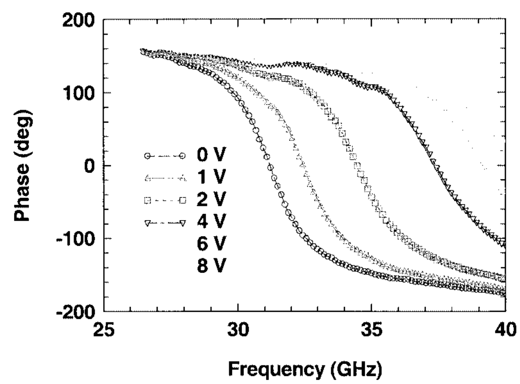

Fig. 7. Measured reflection phase of the InP TQBV tuned EMXT as a function of bias voltage from 0 to 8 V.

able from the equivalent circuit (Fig. 1) since thicker substrate results in higher inductance to capacitance ratio.

B. Tunable EMXT Surfaces

EMXT surfaces with real-time tunable $F_{\rm res}$ can be very attractive in systems requiring frequency and phase agility and multiband multifunctional properties. Either the inductive or the capacitive part of the EMXT structure can be controlled to achieve tunable $F_{\rm res}$. For a particular operating frequency $F_{\rm op}$, an EMXT surface behaves as an inductive surface, a high-impedance surface, and a capacitive surface for $F_{\rm op} < F_{\rm res}$, $F_{\rm op} = F_{\rm res}$, and $F_{\rm op} > F_{\rm res}$, respectively. A tunable EMXT can be used to provide a variable impedance surface through control of $F_{\rm res}$.

In this study, a variable capacitor was chosen to obtain a controlled and variable $F_{\rm res}$ of an EMXT. InP triple quantum barrier varactor (TQBV) was selected and the EMXT was fabricated monolithically on a substrate of semi-insulating InP. The sketch in Fig. 5 illustrates the cross section and equivalent circuit of the devices used to vary the "gap" capacitance. The InP varactor used has a capacitance C–V ranging from 120 to 40 fF when biased with 0 to 10 V and a series resistance Rs of 3 Ω. The polarity of bias was not critical since the TQBV capacitance C–V exhibits an even function of voltage.

A unit-cell design approach was taken since the EMXT can be treated as a two-dimensional periodic structure. Fig. 6 shows a picture of the fabricated EMXT. This EMXT was fabricated on a 200-μm-thick semi-insulating InP substrate with a dielectric constant of 12.5 and loss tangent of 0.002. It has the following geometry: $g = 38$ μm, $w = 410$ μm, via diameter $= 200$ μm, and via periodicity $=$ 508 μm. It was designed to provide a $F_{\rm res}$ that would vary from 30 GHz to above 40 GHz for an applied bias between 0–10 V. The measured reflection phase as a function of frequency at various bias voltages is presented in Fig. 7. The measured tuning range agrees very well with designed values.

The reflection coefficient plotted in Fig. 2 indicates that loss in a passive EMXT is very small, except for substrate modes that occur far away from $F_{\rm res}$. However, for a tunable EMXT, near $F_{\rm res}$, losses associated with the tuning mechanisms are probably the most important loss factor because of the resonant nature of an EMXT structure. The InP TQBV provided an adequate capacitance tuning range for the EMXT, but it exhibited a high series resistance of close to 3 Ω that would give rise to high losses at frequencies near $F_{\rm res}$. The peak reflection loss of the InP EMXT at zero bias is measured to be 7.5 dB. The measured loss is consistent with design predictions and can be attributed mainly to the varactor series resistance Rs. As the biased voltage increases (smaller Cv), EMXT reflection loss decreases accordingly since there is less current flowing through the varactor.

III. EMXT Waveguide Design

Since EMXT surfaces provide useful boundary conditions, they can be used to replace regular metal walls of a waveguide to realize various useful microwave components. The TEM waveguide using EMXT sidewalls have been demonstrated previously [4], [5]. Fig. 8 illustrates the form of an EMXT waveguide. The sidewalls are replaced by the EMXT structure of Fig. 1, making for a totally metal enclosed pipe, but with the inside surface of the sidewalls inhibited from carrying current in the

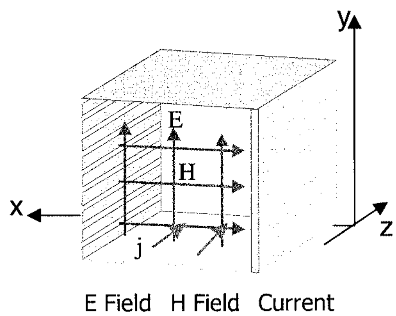

Fig. 8. Schematic drawing of an EMXT waveguide that supports a TEM mode.

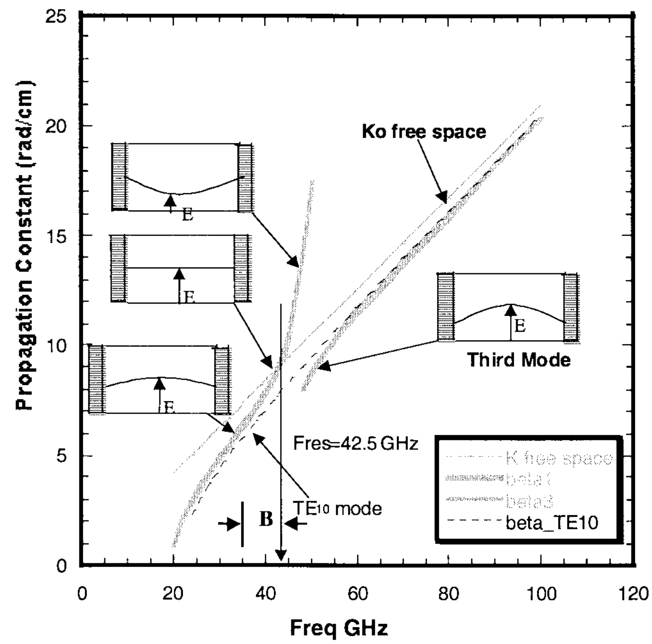

Fig. 9. Calculated propagation modes in an EMXT waveguide of 7-mm width (the EMXT sidewalls are assumed to have an $F_{\rm res}$ of 42.5 GHz).

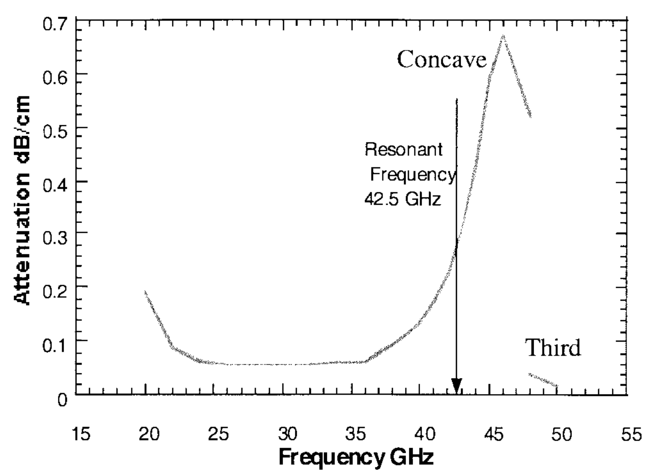

Fig. 10. Calculated attenuation in an EMXT waveguide with an $F_{\rm res}$ of 42.5 GHz.

vertical y-direction at the resonant frequency of the EMXT surfaces. The inability to carry current vertically in the sidewalls affects, at that resonant frequency for which the impedance is highest, the TE modes of the guide converting the TE_{10} mode to a TEM wave inside the pipe. The TEM wave will carry power through this pipe because the necessary currents can flow in the top and bottom surfaces. If the sidewalls were of the polarization insensitive (see [2]) type, i.e., current flow is inhibited in the sidewalls in both the y- and z-directions. In that circumstance, the TE and TM waves are all affected, allowing only the TEM wave to be the dominant mode in the guide at the resonant frequency. Another useful feature of the EMXT guide at resonant frequency is that it has no "cutoff" width and the a, or width dimension, of the waveguide can be arbitrarily small at $F_{\rm res}$ and yet continue to carry a TEM wave.

When implemented with tunable EMXT sidewall surfaces, a very effective and low-loss waveguide phase shifter may be achieved. For example, when $F_{\rm res}$ of the EMXT sidewalls is tuned, the boundary condition of the waveguide sidewalls and, therefore, the propagation constant (β) of the waveguide vary accordingly. To illustrate the EMXT waveguide phase-shifter concept, a simplified waveguide model in which the sidewalls impedance was taken to be that of a parallel $L-C$ circuit (see Fig. 1) was analyzed. Resistances are assigned to L and C to account for losses. $F_{\rm res}$ of the $L-C$ circuit was chosen to be 42.5 GHz. All the conclusions were then confirmed by the results from finite-element simulations. Fig. 9 plots the calculated propagation constant (β) of the TE/TEM modes of the simplified EMXT guide with a width of 7 mm. Propagation in free space and propagation in a normal metal sidewall guide are also depicted by the thin and dashed lines, respectively. The full line shows the propagation of the fundamental TE/TEM mode in the EMXT guide. The characteristic curve of propagation constant β versus the operating frequency $F_{\rm op}$ shows that, when $F_{\rm op}$ coincides with $F_{\rm res}$, the propagation constant is that of free space and the fields (E and H) are uniform inside the guide (illustrated by the inserted cartoon). Power passes through the guide as a TEM wave at that frequency. When $F_{\rm op}$ is below $F_{\rm res}$, the sidewalls have inductive surface impedance increasing with frequency. As $F_{\rm op}$ decreases, the fields relapse slowly to the TE_{10} half-sine, with the maximum field (center) being no more than twice the minimum field (sidewalls) over a bandwidth of 10%. This useful bandwidth "B" (see Fig. 9) depends on the bandwidth of the sidewalls. When $F_{\rm op}$ is above $F_{\rm res}$, the fields at the sidewalls begin to grow and the wavelength decreases rapidly. The field at the sidewalls is nonzero and supported by the capacitive surface impedance of the sidewalls. This impedance is diminishing as the frequency rises and the "concave" (high field at the sidewalls) mode is replaced by a third mode, which gradually becomes more like the TE_{10} mode as $F_{\rm op}$ rises higher above the resonance frequency. This means the dominant mode of propagation in the guide returns to a "TE_{10}-like" state, dubbed in this paper as the "third mode," at a frequency above $F_{\rm res}$.

The useful bandwidth of the EMXT guide is also limited by attenuation, which is depicted in Fig. 10. The computed attenuation is well behaved until $F_{\rm op}$ is above $F_{\rm res}$, at which point the wall current increases and the attenuation rises sharply. Assuming reasonable values for wall metallization resistance and skin effect, i.e., the Q values of L and C in the equivalent circuit of the wall, the attenuation would be below 0.25 dB/cm until

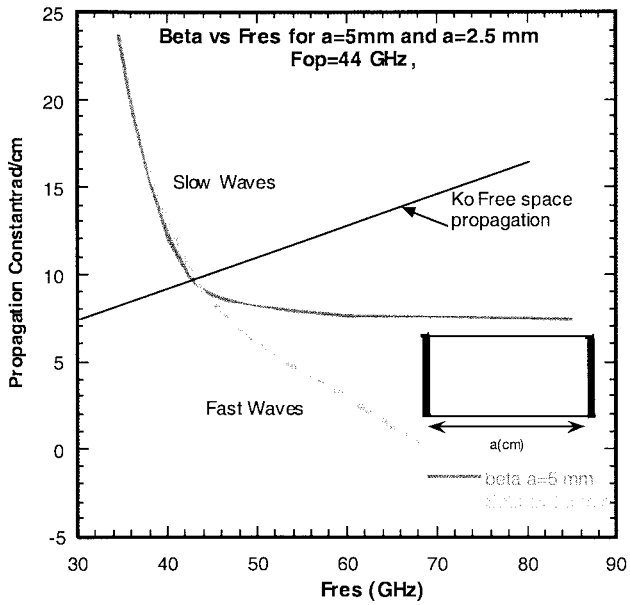

Fig. 11. Calculated dependence of EMXT waveguide propagation constant β on the EMXT sidewall resonance frequency and guide width. The control of phase shift is enhanced for the smaller waveguide width.

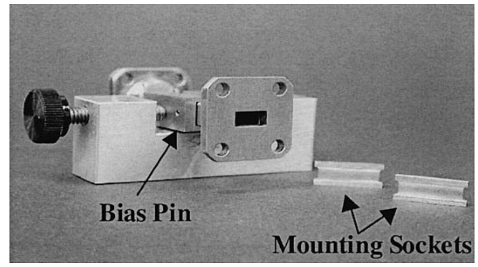

Fig. 12. WR28 waveguide incorporating EMXT sidewalls.

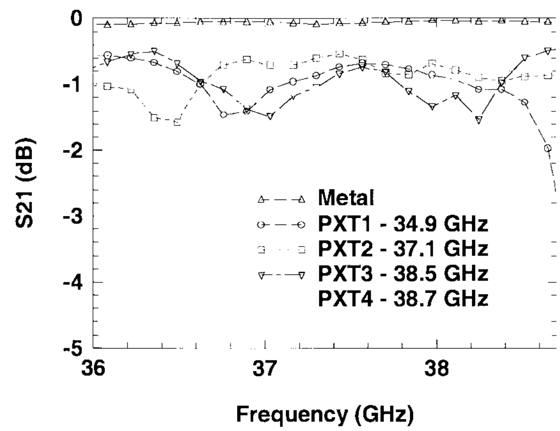

Fig. 13. Measured insertion loss of a 2-cm-long EMXT waveguide with sidewall $F_{\rm res}$ varied by changing fix-tuned EMXT sidewalls. Average insertion losses for all measured fix-tuned EMXT guide are approximately 0.5 dB/cm.

resonance, at which attenuation begins to rise sharply. Above resonance, the attenuation increases until the preferred mode becomes the "third" TE mode.

Fig. 11 illustrates the dependence of propagation constant β of an EMXT waveguide with a width of 5 and 2.5 mm on the resonance frequency $F_{\rm res}$ of the sidewalls for a fixed $F_{\rm op} =$ 44 GHz. It is apparent that the phase shift of a fixed-length EMXT waveguide can be controlled effectively by varying the $F_{\rm res}$ of the sidewalls. This controlling influence is stronger for the slow-wave region ($F_{\rm res} < F_{\rm op}$) than for the fast-wave region. However, there is a probability of elevated losses exists in the slow-wave region.

The effectiveness of phase control also depends on the size of an EMXT waveguide phase shifter. From Fig. 11, it can be seen that the control of phase shift for the fast-wave region is enhanced for smaller waveguide width. Thus, a very effective phase shifter is possible for 44 GHz if the guide width is 2.5 mm (instead of 5 mm), and the resonant frequency may be changed from 44 up to 50 GHz. One physical way to look at the EMXT waveguide is that the EM wave traveling inside the guide bounces back and forth off the EMXT sidewalls and each reflection introduces a phase shift depending on the $F_{\rm res}$ of the sidewalls. For a smaller width guide, there will be more reflections on the sidewalls than that of a greater width guide. Thus, phase shifting per unit length for the EMXT waveguide increases as its width decreases. These ideas for an effective phase shifter to work with the waveguide enclosed array amplifiers [10] have been the impetus to follow an experimental inquiry into these EMXT-based waveguides.

IV. EMXT Waveguide Results

A. EMXT Waveguide Assembly

The experimental waveguides of this study had a guide width of 7 mm, as they were adapted from a WR28 metal guide by the removal of the metal sidewalls and their replacement by the EMXT structures. EMXT surfaces described in Section II are mounted into two brass sockets, as shown in Fig. 12. The two brass sockets are then clamped to the sides of a WR28 waveguide with its sidewalls removed. Both the fix-tuned EMXT and InP TQBV-tuned EMXT waveguide were made and measured. For the TQBV-tuned EMXT waveguide, the bias of varactors was achieved by biasing adjacent metal strips on the front side of EMXT with wire bonds.

B. Fix-Tuned EMXT Waveguide

Initial Ka-band EMXT waveguides were fixed tuned, i.e., they did not contain tunable sidewalls using varactors, but had EMXT sidewalls of fixed resonant frequencies. These fixed EMXT surfaces were fabricated on a Rogers Duroid substrate (RO3006) of relative dielectric constant 6.15 and a loss tangent of 0.013 at 35 GHz. The substrates were 0.62-mm thick and copper coated on both sides, with patterns etched on one side. The patterns were slots that formed strips on the inner sidewall of the waveguides, as shown in Fig. 8. Plated through substrate vias were included in the design and fabrication. The EMXT samples used have $F_{\rm res}$ of 34.6, 37.1, 38.5, and 38.7 GHz. Transmission measurements were made of millimeter-wave signals, at frequencies between 36–39 GHz, propagating through 2 cm of the 7-mm-wide EMXT waveguide. Results are plotted in Fig. 13. The insertion loss is approximately 0.5 dB per cm for the EMXT guides and shows no discernable maximal near $F_{\rm res}$. The insertion loss is compared against that of an empty guide. This 0.5 dB/cm is a tolerable level

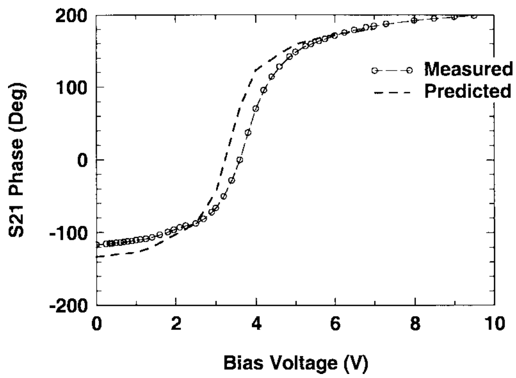

(a)

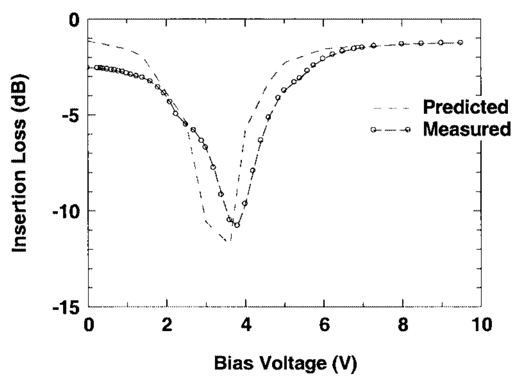

(b)

Fig. 14. Measured (circled line) and predicted (dashed line) EMXT waveguide: (a) phase shift and (b) insertion loss as a function of bias voltage at 38 GHz.

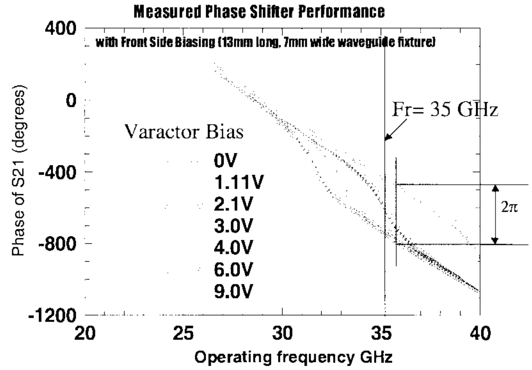

Fig. 15. Control of phase achieved with an InP TQBV-based EMXT waveguide over the entire Ka-band.

of insertion loss and can be reduced by further design and materials optimization (e.g., reduction of loss tangent).

It is noticeable that the sharp rise of the insertion loss, expected as operating frequency exceeds resonant frequency (as shown in Fig. 10), is not apparent. The expected rise in insertion loss depends upon the "concave mode" above resonance; i.e., that mode which enhances the fields at the sidewalls and currents in the sidewall metals, which cause the increase in loss. The Duroid fixed-tuned sidewalls with their moderately high dielectric loss (a loss tangent of 0.013) appear to show little or no influence of the "concave mode" and show dielectric losses, which indicate a rapid conversion to the TE_{10}-like "third-mode." At 38 GHz, approximately 60° of $S21$ phase change is measured for this fixed-tuned EMXT waveguide with sidewalls of F_{res} from 34.6 to 38.7 GHz.

C. Tunable EMXT Phase Shifter

InP TQBV tuned EMXT described in Section II was used to implement a Ka-band waveguide phase shifter. From the reflection characteristics of the tunable EMXT, the waveguide phase shifter incorporating EMXT sidewalls can be modeled by the finite-element method quite accurately with an effective surface impedance approach. Fig. 14 compares the measured and predicted phase-shifter performance as a function of bias voltage at 38 GHz. The agreement between measured and designed phase shift and insertion loss is very well. For the 13-mm-long 7-mm-wide (WR28) InP TQBV EMXT waveguide measured, a total of approximately 320° of phase shift was achieved with less than 10 V of biasing.

The insertion loss in this demonstration was high, peaking at approximately 10 dB, while the average loss is approximately 6 dB. The insertion loss peaks up at frequencies a little higher than F_{res}, as explained in Fig. 10. As mentioned previously, both simulations and measurements have confirmed that the loss is mainly due to the varactor series resistance Rs. This high resistance has been addressed in the following designs, and the expected maximum loss is approximately 2 dB in optimized full-wave EMXT waveguide phase-shifter designs that use GaAs Schottky diodes instead of InP TQBV as the tuning devices.

The phase control of this 7-mm-wide EMXT waveguide phase shifter over the entire Ka-band is plotted in Fig. 15. For less than 10 V of bias voltage, this EMXT guide achieved a nearly 2π-phase shift from 32 to 40 GHz and above.

One of the concerns for this new type of phase shifter is its nonlinearity caused by the RF-signal modulation. The third-order intermodulation distortion (IMD) of the InP TQBV-tuned EMXT phase shifter was characterized using the standard two-tone method. At 38 GHz, no IMD signal above the equipment noise floor was observed for the highest input signals available. A lower limit of the third order intercept (IP3) was +36 dBm, which is satisfactory. Enhancement of linearity can be achieved by designing and incorporating varactors with optimized C–V characteristics.

Since smaller EMXT waveguide size may lead to more efficient phase shifter (see Fig. 11), a 10-mm-long 3-mm-wide waveguide with the same EMXT sidewalls was designed and fabricated to achieve 360° of phase shift. A four-by-four phased array has been demonstrated using 16 such 3-mm-wide InP TQBV EMXT waveguide as both the phase-shifting and radiating elements [13].

V. Discussion and Conclusions

A new type of millimeter-wave waveguide phase shifter using tunable EMXT surfaces as sidewalls has been demonstrated. The key aspect of attaining performance is the implementation of a low-loss tuning system that will vary the waveguide sidewall impedance. The design and fabrication of EMXT waveguides in which the sidewall impedance values are continuously tuned, either by varactor systems built into the sidewall or by microelectromechanical systems (MEMS) built into the sidewall, will provide, following optimization, phase-shifting waveguides that will be compatible with phased-array antennas and quasi-optical amplifiers applications. Other methods that are currently being evaluated and that simplify the realization of tuning capability are the substitution of control over the substrate dielectric constant (ferroelectric materials) or the substrate permeability (ferrite materials).

Experimental results of the EMXT waveguide phase shifters that are in development show promise of effectiveness and low loss. Design optimization will enable realization of a guide to achieve a phase shift of 2π rad and a loss less than 2 dB with a length of 10 mm at 38 GHz. These devices working with quasi-optical amplifiers mounted will provide an innovative way to extract power performance from solid-state amplifiers at millimeter waves up to and over 100 GHz. In addition, these devices will provide an innovative alternative in the area of advanced electronically steered antenna systems.

ACKNOWLEDGMENT

The authors would like to thank G. Nagy and R. Pittman, both of the Rockwell Scientific Company, Thousand Oaks, CA, for their expert assistance in the fabrication process. The authors are also grateful for technical discussions with J. B. Hacker, Rockwell Scientific Company, and M. Kim, Korea University, Seoul, Korea.

REFERENCES

[1] D. Sievepiper, "High impedance electromagnetic surfaces," Ph.D. dissertation, Dept. Elect. Eng., UCLA, Los Angeles, CA, 1998.
[2] D. Sievenpiper, R. Broas, and E. Yablonovitch, "Antennas on high-impedance ground planes," in *IEEE MTT-S Int. Microwave Symp. Dig.*, June 1999, pp. 1245–1248.
[3] H. Xin *et al.*, "Mutual coupling of monopole antennas on high impedance ground plane," *Electron. Lett.*, vol. 38, no. 16, pp. 849–850, Aug. 2002.
[4] J. A. Higgins *et al.*, "The application of photonic crystals to quasi-optic amplifiers," *IEEE Trans. Microwave Theory Tech.*, vol. 47, pp. 2139–2143, Nov. 1999.
[5] F. R. Yang, K. P. Ma, Y. Qian, and T. Itoh, "A novel TEM waveguide using uniplanar compact photonic-bandgap (UC-PBG) structure," *IEEE Trans. Microwave Theory Tech.*, vol. 47, pp. 2092–2098, Nov. 1999.
[6] C. Kariazidou, H. F. Contopanagos, and N. G. Alexopoulos, "Monolithic waveguide filters using printed photonic-bandgap materials," *IEEE Trans. Microwave Theory Tech.*, vol. 49, pp. 297–307, Feb. 2001.
[7] S. T. Chew and T. Itoh, "PBG-excited split-mode resonator bandpass filter," *IEEE Microwave Guided Wave Lett.*, vol. 11, pp. 364–366, Sept. 2001.
[8] D. Sievenpiper *et al.*, "Electronic beam steering using a varactor-tuned impedance surface," in *IEEE AP-S Int. Symp. Dig.*, vol. 1, June 2001, pp. 174–177.
[9] J. A. Higgins, H. Xin, and A. Sailer, "Characteristics of Ka-band waveguide using electromagnetic crystal sidewalls," in *IEEE MTT-S Int. Microwave Symp. Dig.*, 2002, pp. 1071–1074.
[10] M. Kim *et al.*, "A rectangular TEM waveguide with photonic crystal walls for excitation of quasioptic amplifiers," in *IEEE MTT-S Int. Microwave Symp. Dig.*, 1999, pp. 543–546.
[11] W. W. Anderson, "Mode confinement and gain in junction lasers," *IEEE J. Quantum Electron.*, vol. QE-1, pp. 228–236, Sept. 1965.
[12] I. P. Kaminow *et al.*, "Metal clad optical waveguides: Analytical and experimental study," *Appl. Opt.*, vol. 13, no. 2, pp. 396–405, Feb. 1974.
[13] J. West *et al.*, "A two dimensional millimeter wave phase scanned lens utilizing analog photonic bandgap waveguide phase shifters," presented at the Allerton Antenna Applications Symp., Sept. 2002.

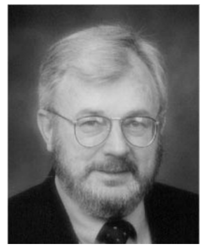

J. Aiden Higgins received the B.E. from the University of California at Davis, Davis, in 1958, the M.S.E.E. and Ph.D. degrees in electrical engineering from Stanford University, Stanford, CA, in 1964, and 1971, respectively.

Upon graduation, he joined the Rockwell Science Company (RSC), Thousand Oaks, CA, where he was involved with the development of GaAs MESFETs. During the 1970s, he was a leading contributor to the development of the ion-implanted MESFET, demonstrating that the device provided excellent low-noise and linear power performance. This work ultimately led to the earliest monolithic microwave integrated circuits (MMICs) and integrated circuits for digital application. During the 1980s, he led and managed the RSC development of GaAs-based charge-coupled devices (CCDs) for high-speed signal processing and GaAs-based high electron-mobility transistor (HEMT) MMICs for millimeter-wave low-noise amplification and power. In the late 1980s and the 1990s, he was the leader and Manager of the development of the GaAs HBT power-amplifier technology; a technology that currently finds commercial application in wireless communication systems. His more recent research has included the development of spatial power-combining methods and novel transmission media for millimeter waves, which will make available multiwatt levels of power at frequencies above 35 GHz. He is currently a Principal Scientist with RSC, where he contributes to the application of new technologies such as photonic crystals and gallium–nitride devices to tasks in microwave and millimeter systems. He has authored or coauthored over 90 technical papers appearing in the professional journals. He holds nine patents with two pending.

Hao Xin (M'01) received the B.S. degree in mathematics and physics from the University of Massachusetts at Dartmouth, in 1995, and the Ph.D. degree in physics from the Massachusetts Institute of Technology (MIT), Cambridge, in 2001.

He possesses five years of research experience with the Physics Department, Lincoln Laboratory, Analog Device Group, MIT, and Air Force Research Laboratory (AFRL), Hanscom AFB, where he has been involved with power dependence of the surface impedance of high-Tc superconducting films at microwave frequencies and cryogenic temperatures in order to make better microwave devices for communication applications. Since November 2000, he has been a Research Scientist with the RSC, where his current efforts focus on EM bandgap surfaces at microwave and millimeter-wave frequencies, quasi-optical devices, electronically scanned antenna arrays, and MMIC designs using GaAs pseudomorphic high electron-mobility (pHEMT) technology. He has authored or coauthored various technical papers on topics including microwave superconductivity, Josephson junctions, EM bandgap surfaces, and their applications in microwave and millimeter-wave components and systems.

A. Sailer, photograph and biography not available at time of publication.

Mark Rosker received the B.S. degree in physics from the California Institute of Technology, Pasadena, in 1981, and the M.S. and Ph.D. degrees in applied and engineering physics from Cornell University, Ithaca, NY, in 1983 and 1987, respectively. His doctoral research was divided between the areas of nonlinear optics, including the development of a urea optical parametric oscillator, and ultrafast phenomena, in which the femtosecond energy relaxation of semiconductors and organic molecules were investigated.

He is currently Manager of the RF Circuits and Applications Department, Rockwell Scientific Company (RSC), Thousand Oaks, CA, and Director of the Collins Programs. From 1986 to 1989, he was a Post-Doctoral Research Fellow with the California Institute of Technology, where he performed fundamental studies (which was cited in the 1999 Nobel Prize in chemistry) observing the dynamics of unimolecular chemical reactions in real time. In 1989, he joined the Applied Optics Department, RSC, and contributed significantly to research projects in nonlinear optics, including photorefractive oscillators and visible and infrared frequency conversion materials and devices, time-domain spectroscopy of optical materials, and optical power limiters. He subsequently joined and eventually became the Manager of the Device Chemistry Department, Materials Science Division, RSC, performing further research in optical materials, as well as the study of advanced energy storage devices. In 1999, he became the Manager of the Microwave and Photonics Department (now called the RF Circuits and Applications), Electronics Division, RSC. This group is well known for its pioneering development of quasi-optics and other novel III–V devices, including high-performance GaAs pHEMT and InP HEMT technologies for MMIC amplifiers, mixers, and antennas. Its photonics efforts have focused on optical holographic storage and processing, nonlinear materials, and, more recently, optical techniques for accomplishing RF beamforming. In addition to these responsibilities, since 1996, he has acted as the primary liaison between Rockwell Collins and the RSC. As such, he has been responsible for the planning and oversight of the research and development portfolio of all research programs sponsored by Rockwell Collins at the RSC and with maintaining a mutually productive relationship with one of RSC's largest customers. He has authored over 70 technical papers and conference proceedings.